symmetry

IMPACT FACTOR 2.7

CITESCORE 4.9

Review

Spherical, Axial, and Triaxial Symmetries in the Study of Halo Nuclei with Covariant Density Functional Theory

Yifeng Xiang, Qingjin Luo, Siqi Yang and Kaiyuan Zhang

Special Issue
Role of Symmetries in Nuclear Physics

Edited by
Prof. Dr. Peter Otto Hess

MDPI

https://doi.org/10.3390/sym15071420

symmetry

MDPI

Review

Spherical, Axial, and Triaxial Symmetries in the Study of Halo Nuclei with Covariant Density Functional Theory

Yifeng Xiang [1], Qingjin Luo [1], Siqi Yang [2,*] and Kaiyuan Zhang [1,*]

[1] Institute of Nuclear Physics and Chemistry, China Academy of Engineering Physics, Mianyang 621900, China
[2] Institute of Computer Application, China Academy of Engineering Physics, Mianyang 621900, China
* Correspondence: yangsiqi@caep.cn (S.Y.); zhangky@caep.cn (K.Z.)

Abstract: The halo phenomenon in exotic nuclei has long been an important frontier in nuclear physics research since its discovery in 1985. In parallel with the experimental progress in exploring halo nuclei, the covariant density functional theory has become one of the most successful tools for the microscopic study of halo nuclei. Based on spherical symmetry, the relativistic continuum Hartree–Bogoliubov theory describes the first halo nucleus ^{11}Li self-consistently and predicts the giant halo phenomenon. Based on axial symmetry, the deformed relativistic Hartree–Bogoliubov theory in continuum has predicted axially deformed halo nuclei ^{42,44}Mg and the shape decoupling effects therein. Based on triaxial symmetry, recently the triaxial relativistic Hartree–Bogoliubov theory in continuum has been developed and applied to explore halos in triaxially deformed nuclei. The theoretical frameworks of these models are presented, with the efficacy of exploiting symmetries highlighted. Selected applications to spherical, axially deformed, and triaxially deformed halo nuclei are introduced.

Keywords: halo nuclei; covariant density functional theory; spherical symmetry; axial symmetry; triaxial symmetry

Citation: Xiang. Y.; Luo, Q.; Yang, S.; Zhang, K. Spherical, Axial, and Triaxial Symmetries in the Study of Halo Nuclei with Covariant Density Functional Theory. *Symmetry* **2023**, *15*, 1420. https://doi.org/10.3390/sym15071420

Academic Editor: Peter Otto Hess

Received: 30 June 2023
Revised: 12 July 2023
Accepted: 13 July 2023
Published: 14 July 2023

1. Introduction

In 1985, Tanihata et al. [1] found a significant increase in the radius of ^{11}Li compared to ^{9}Li, which may correspond to an abnormal neutron distribution. In 1988, Kobayashi et al. [2] discovered that the width of the transverse-momentum distributions of the two outer neutrons in ^{11}Li is extremely narrow, indicating their highly diffuse spatial distribution. Thus, the exotic structure of ^{11}Li was revealed; two neutrons are loosely bound around the core of ^{9}Li, forming a dilute neutron matter over a large spatial range. This novel phenomenon is popularly referred to as a "neutron halo".

The unprecedented low-density neutron matter has shaken the fundamental assumption in nuclear physics—the incompressibility of nuclear matter. The radii of halo nuclei largely deviate from the empirical formula of $r_0 A^{1/3}$, in which $r_0 \approx 1.2$ fm and A is the mass number. As a result, the halo phenomenon rapidly attracted lots of research interest. The relevant studies have not only propelled the worldwide development of radioactive ion beam facilities but also advanced the improvement of nuclear models.

Further experiments have revealed the signals of halo phenomena in nuclei other than ^{11}Li, including proton halo nuclei near the proton dripline. The identification of a halo nucleus typically entails the observation of both an increased reaction cross section and a narrow momentum distribution of reaction fragments [3]. However, the presence of either one of these characteristics, along with other relevant signals, can also indicate a potential halo candidate. To date, a total of 13 halo nuclei have been identified, and experimental investigations have proposed 10 candidates, as depicted in Figure 1.

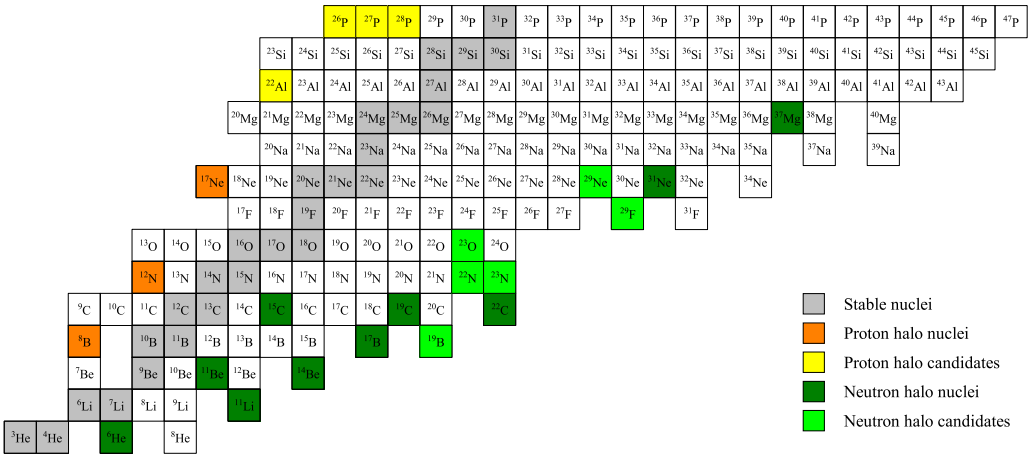

Figure 1. Experimentally known nuclear landscape from helium to phosphorus, where stable nuclei and experimentally confirmed/suggested neutron as well as proton halo nuclei/candidates are indicated in gray, olive/green, and orange/yellow colors, respectively. Taken from Ref. [4].

On the theoretical side, numerous models have been employed to investigate halo nuclei, including the few-body model [5,6], shell model [7,8], antisymmetrized molecular dynamics [9,10], halo effective field theory [11,12], and density functional theory [13,14]. Among these, nuclear density functional theory has emerged as a comprehensive framework for studying the properties of almost all nuclei across the nuclear landscape [15]. Its relativistic counterpart, known as covariant density functional theory (CDFT), possesses distinct advantages, such as the automatic inclusion of the spin degree of freedom and the spin–orbital interaction [16], the explanation of the pseudospin symmetry in the nucleon spectrum [17–22] and the spin symmetry in the antinucleon spectrum [22–24], the natural inclusion of the nuclear magnetism [25], etc. As a result, the CDFT has garnered considerable attention and has been successfully employed to describe the ground-state and excited-state properties of atomic nuclei [26–33].

Symmetry breaking is an essential element of nuclear density functional theory. The intrinsic nuclear density can break some symmetries that characterize the nuclear Hamiltonian. One prominent example is the spontaneous breaking of symmetry within the mean field, which gives rise to the concept of nuclear deformation. In other words, the intrinsic density distribution of a nucleus can be non-spherical, incorporating important correlations into the mean-field wave function in an economical manner. The notion of nuclear deformation has proven valuable in interpreting many low-lying excited states [34]. In many investigations, one usually begins with a mean-field solution that assumes spatial symmetry, and subsequently restores any broken symmetries as necessary using projection methods, such as the angular momentum projection (AMP) technique.

The pairing interaction in weakly bound nuclei can scatter nucleons from bound states to continuum states. This coupling to the continuum can lead to a more diffuse density distribution, and the location of the dripline might be affected. Therefore, in the study of halo nuclei, it is essential to consider not only the nuclear shape dominated by the mean field, but also the important roles played by pairing correlations and continuum effects.

Based on the CDFT, assuming spherical symmetry and self-consistently considering the pairing correlations and continuum effects, the relativistic continuum Hartree–Bogoliubov (RCHB) theory is capable of describing spherical halo nuclei [14,35]. The RCHB theory provided a microscopic description of the neutron halo in ^{11}Li [14], predicted the existence of giant halos [36], and explored the halo phenomena in hypernuclei [37]. Recently, the first relativistic nuclear mass table incorporating the continuum effects has been constructed based on the RCHB theory [38].

Except for doubly magic nuclei, most nuclei exhibit deviations from a spherical shape. To adequately describe deformed halo nuclei, the deformed relativistic Hartree–Bogoliubov theory in continuum (DRHBc) has been developed [39–42]. The DRHBc theory not only inherits the advantageous treatment of pairing correlations and continuum effects from the RCHB theory but also incorporates the axial deformation degrees of freedom by assuming axial symmetry. The success of the DRHBc theory for nuclear halos was demonstrated in the description of halo phenomena in ^{17,19}B [43,44], ^{15,19,22}C [45,46], and ^{31}Ne [47] as well as the prediction of deformed halo nuclei ^{39}Na [4] and ^{42,44}Mg [39,40,48]. Currently, efforts are underway to construct a nuclear mass table that incorporates both deformation and continuum effects based on the DRHBc theory [49–54].

Deviations from axial symmetry in the intrinsic density, known as triaxial distributions, are of significant interest in enhancing the understanding of the mechanisms underlying nuclear deformation. Recently, the triaxial relativistic Hartree–Bogoliubov theory in continuum (TRHBc) has been developed, which incorporates the triaxial deformation degrees of freedom, pairing correlations, and continuum effects in a microscopic and self-consistent way [55]. The TRHBc theory has explored the existence of triaxially deformed halo nuclei and predicted ^{42}Al to be a candidate [55].

This paper is organized as follows. Section 2 presents the basic framework of the CDFT and shows how symmetry simplifies the formalism of the RCHB, DRHBc, and TRHBc theories. Section 3 introduces the background of the development of these theories and their first applications to spherical, axially deformed, and triaxially deformed halo nuclei. Section 4 gives a summary.

2. Symmetries in the CDFT for Halo Nuclei

2.1. Basic Framework of the CDFT

Taking the point-coupling density functional as an example, the CDFT starts from the Lagrangian density [56]

$$\begin{aligned}\mathcal{L} =&\bar{\psi}(i\gamma_\mu\partial^\mu - M)\psi - \frac{1}{2}\alpha_S(\bar{\psi}\psi)(\bar{\psi}\psi) - \frac{1}{2}\alpha_V(\bar{\psi}\gamma_\mu\psi)(\bar{\psi}\gamma^\mu\psi) - \frac{1}{2}\alpha_{TV}(\bar{\psi}\vec{\tau}\gamma_\mu\psi)(\bar{\psi}\vec{\tau}\gamma^\mu\psi)\\ &- \frac{1}{2}\alpha_{TS}(\bar{\psi}\vec{\tau}\psi)(\bar{\psi}\vec{\tau}\psi) - \frac{1}{3}\beta_S(\bar{\psi}\psi)^3 - \frac{1}{4}\gamma_S(\bar{\psi}\psi)^4 - \frac{1}{4}\gamma_V[(\bar{\psi}\gamma_\mu\psi)(\bar{\psi}\gamma^\mu\psi)]^2\\ &- \frac{1}{2}\delta_S\partial_\nu(\bar{\psi}\psi)\partial^\nu(\bar{\psi}\psi) - \frac{1}{2}\delta_V\partial_\nu(\bar{\psi}\gamma_\mu\psi)\partial^\nu(\bar{\psi}\gamma^\mu\psi) - \frac{1}{2}\delta_{TV}\partial_\nu(\bar{\psi}\vec{\tau}\gamma_\mu\psi)\partial^\nu(\bar{\psi}\vec{\tau}\gamma^\mu\psi)\\ &- \frac{1}{2}\delta_{TS}\partial_\nu(\bar{\psi}\vec{\tau}\psi)\partial^\nu(\bar{\psi}\vec{\tau}\psi) - \frac{1}{4}F^{\mu\nu}F_{\mu\nu} - e\bar{\psi}\gamma^\mu\frac{1-\tau_3}{2}A_\mu\psi,\end{aligned} \tag{1}$$

where M is the nucleon mass, e is the charge unit, A_μ and $F_{\mu\nu}$ are, respectively, the four-vector potential and field strength tensor of the electromagnetic field, and α, β, γ, and δ represent the coupling constants for different channels with the subscripts S, V, and T standing for scalar, vector, and isovector, respectively. The isovector-scalar channel including the terms α_{TS} and δ_{TS} in Equation (1) are usually neglected since they do not improve the description of nuclear ground-state properties [57].

The energy density functional can be constructed by assuming the ground-state wave function as the quasiparticle vacuum

$$|\Phi\rangle = \prod_k \beta_k|0\rangle, \tag{2}$$

where $|0\rangle$ is the bare vacuum and β_k is the quasiparticle annihilation operator. The quasiparticle operators $\beta_k^\dagger$ and β_k are defined by a unitary Bogoliubov transformation from particle operators $c_l^\dagger$ and c_l of an arbitrary complete and orthogonal basis,

$$\beta_k^\dagger = \sum_l (U_{lk}c_l^\dagger + V_{lk}c_l), \tag{3}$$

where U and V are quasiparticle wave functions.

The variation in the energy density functional leads to the relativistic Hartree–Fock–Bogoliubov equation,

$$\begin{pmatrix} \hat{h}_D - \lambda_\tau & \hat{\Delta} \\ -\hat{\Delta}^* & -\hat{h}_D^* + \lambda_\tau \end{pmatrix} \begin{pmatrix} U_k \\ V_k \end{pmatrix} = E_k \begin{pmatrix} U_k \\ V_k \end{pmatrix}, \tag{4}$$

which treats the nuclear mean field and pairing correlations on the same footing. In most cases, only the Hartree (direct) terms are considered, and the Fock (exchange) terms are neglected by assuming that their effects could be absorbed in the adjustments of the coupling constants of energy density functionals. This paper will also be limited to the relativistic Hartree–Bogoliubov (RHB) framework. Details on the relativistic Hartree–Fock–Bogoliubov theory and its applications can be found in Refs. [58–60].

In Equation (4), $\hat{h}_D$ is the Dirac Hamiltonian, $\hat{\Delta}$ is the pairing field, λ_τ is the Fermi surface for the neutron or proton ($\tau = n$ or p), and E_k is the quasiparticle energy. The Dirac Hamiltonian reads

$$h_D(\boldsymbol{r}) = \boldsymbol{\alpha} \cdot \boldsymbol{p} + V(\boldsymbol{r}) + \beta[M + S(\boldsymbol{r})], \tag{5}$$

with the scalar and vector potentials

$$S(\boldsymbol{r}) = \alpha_S \rho_S + \beta_S \rho_S^2 + \gamma_S \rho_S^3 + \delta_S \Delta\rho_S, \tag{6}$$

$$V(\boldsymbol{r}) = \alpha_V \rho_V + \gamma_V \rho_V^3 + \delta_V \Delta\rho_V + eA^0 + \alpha_{TV} \tau_3 \rho_3 + \delta_{TV} \tau_3 \Delta\rho_3, \tag{7}$$

constructed by various densities

$$\begin{aligned} \rho_S(\boldsymbol{r}) &= \sum_{k>0} V_k^\dagger(\boldsymbol{r}) \gamma_0 V_k(\boldsymbol{r}), \\ \rho_V(\boldsymbol{r}) &= \sum_{k>0} V_k^\dagger(\boldsymbol{r}) V_k(\boldsymbol{r}), \\ \rho_3(\boldsymbol{r}) &= \sum_{k>0} V_k^\dagger(\boldsymbol{r}) \tau_3 V_k(\boldsymbol{r}). \end{aligned} \tag{8}$$

The pairing field is

$$\Delta(\boldsymbol{r}_1, \boldsymbol{r}_2) = V^{pp}(\boldsymbol{r}_1, \boldsymbol{r}_2) \kappa(\boldsymbol{r}_1, \boldsymbol{r}_2), \tag{9}$$

where the spin and isospin degrees of freedom are not shown for simplicity, V^{pp} is the pairing force, and κ is the pairing tensor [61]. In the CDFT, a zero-range density-dependent force and a finite-range Gogny or separable force are usually employed in the pairing channel [35,62,63].

After the RHB equation is iteratively solved, one can calculate the total energy of a nucleus by

$$\begin{aligned} E_{\mathrm{RHB}} = &\sum_{k>0} (\lambda_\tau - E_k) v_k^2 - E_{\mathrm{pair}} \\ &- \int \mathrm{d}^3\boldsymbol{r} \Big(\frac{1}{2}\alpha_S \rho_S^2 + \frac{1}{2}\alpha_V \rho_V^2 + \frac{1}{2}\alpha_{TV} \rho_3^2 \\ &+ \frac{2}{3}\beta_S \rho_S^3 + \frac{3}{4}\gamma_S \rho_S^4 + \frac{3}{4}\gamma_V \rho_V^4 + \frac{1}{2}\delta_S \rho_S \Delta\rho_S \\ &+ \frac{1}{2}\delta_V \rho_V \Delta\rho_V + \frac{1}{2}\delta_{TV} \rho_3 \Delta\rho_3 + \frac{1}{2}\rho_p e A^0 \Big), \end{aligned} \tag{10}$$

where

$$v_k^2 = \int d^3\boldsymbol{r} V_k^\dagger(\boldsymbol{r}) V_k(\boldsymbol{r}), \tag{11}$$

and

$$E_{\mathrm{pair}} = \mathrm{Tr}(\Delta\kappa) \tag{12}$$

is the pairing energy. The root-mean-square (rms) radius is calculated as

$$R_{\rm rms} = \langle r^2 \rangle^{1/2} = \sqrt{\frac{\int r^2 \rho_v(\boldsymbol{r}) d^3\boldsymbol{r}}{\int \rho_v(\boldsymbol{r}) d^3\boldsymbol{r}}}. \tag{13}$$

The intrinsic quadrupole moments are calculated as

$$\begin{aligned} Q_{20} &= \langle r^2 Y_{20} \rangle = \int r^2 Y_{20} \rho_v(\boldsymbol{r}) d^3\boldsymbol{r}, \\ Q_{22} &= \frac{1}{2} \langle r^2 (Y_{22} + Y_{2-2}) \rangle = \frac{1}{2} \int r^2 (Y_{22} + Y_{2-2}) \rho_v(\boldsymbol{r}) d^3\boldsymbol{r}, \end{aligned} \tag{14}$$

which can be used to extract the deformation parameters β and γ of a nucleus. For spherical nuclei, $\beta = 0$ and $\gamma = 0$. For axially deformed nuclei, $\gamma = 0$ and the quadrupole deformation parameter β_2 is commonly used instead of β. For triaxially deformed nuclei, both β and γ take nonzero values.

The single-particle levels in the canonical basis $|\psi_i\rangle$ are very useful to study the nuclear properties in a microscopic way. These are eigenstates of the density matrix $\hat{\rho} = V^* V^{\rm T}$ and the corresponding eigenvalues are their occupation probabilities [61]. In general, $|\psi_i\rangle$ is not an eigenstate of the Dirac Hamiltonian $\hat{h}_D$. The expectation value $\langle \psi_i | \hat{h}_D | \psi_i \rangle$ is referred to as its single-particle energy.

2.2. Solving the RHB Equation

Solving the RHB equation is usually transformed into a matrix diagonalization problem in the harmonic oscillator (HO) basis [64], because the HO potential can be easily solved and the analytical form of the HO wave function can bring some convenience in the matrix element calculation. However, due to the incorrect asymptotic behavior of HO wave functions, the expansion in a localized HO basis is incapable of describing weakly bound nuclei with diffuse spatial density distributions, e.g., halo nuclei. To improve the asymptotic behavior of HO wave functions, a transformed HO basis has been proposed in Refs. [65,66] via a local scaling transformation.

Solutions in coordinate space can properly describe the asymptotic behavior of wave functions. For nuclei with small separation energies, the coordinate-space calculations in large boxes are found to be more effective than the transformed HO basis [67]. However, only the RHB equation assuming spherical symmetry has been solved in coordinate space [14,68]. Solving the deformed RHB equation in coordinate space is extremely difficult if not impossible [69].

A Woods–Saxon basis, whose wave function has an appropriate asymptotic behavior, was proposed as a reconciler between the HO basis and coordinate space [70]. It is obtained by solving the Schrödinger equation or the Dirac equation containing spherical Woods–Saxon potentials with box boundary conditions, and is correspondingly referred to as the Schrödinger Woods–Saxon (SWS) or the Dirac Woods–Saxon (DWS) basis. For spherical nuclei, the solution of the relativistic Hartree equations in the SWS or DWS basis is found to be almost equivalent to that in coordinate space [70]. However, the DWS basis expansion is more straightforward in the CDFT because there is no need to expand the upper and lower components of the relativistic wave function separately. It turns out that the DWS basis expansion is more efficient than the SWS one in solving the relativistic Hartree equations [70]. Both SWS and DWS bases have been widely applied to various nuclear models to study weakly bound nuclei [58–60,71,72]. Recently, an optimized DWS basis whose corresponding potential is close to the nuclear mean field is proposed, and its basis space required for convergence is substantially reduced compared to the original one [73].

The wave function of the DWS basis can be written as

$$|n\kappa m\rangle = i^p \frac{R_{n\kappa}(r,p)}{r} \mathcal{Y}^{l(p)}_{\kappa m}(\Omega, s), \tag{15}$$

where n, κ, and m are its quantum numbers, which will be introduced below. $\boldsymbol{r}$, s, and p are the spatial coordinate, spin, and index ($p = 1$ or 2) for the upper or lower component, respectively. $R_{n\kappa}$ is the radial wave function and n is its node number. $\mathcal{Y}^l_{\kappa m}$ is the spinor spherical harmonic,

$$\mathcal{Y}^l_{\kappa m}(\Omega, s) = \sum_{m_l, m_s} \langle \frac{1}{2} m_s l m_l | j m \rangle Y_{l m_l}(\Omega) \chi_{\frac{1}{2} m_s}(s), \tag{16}$$

where $Y_{l m_l}$ is the spherical harmonic function, $\chi_{\frac{1}{2} m_s}$ is the spin wave function, l is the orbital angular momentum, j is the total angular momentum, and m_l, m_s, and m are the third components of l, s, and j, respectively. The quantum number κ is given by the parity π and j, $\kappa = \pi(-1)^{j+1/2}(j + 1/2)$. The orbital angular momenta for upper and lower components are

$$l(1) = j + \frac{1}{2}\mathrm{sgn}(\kappa), \;\; l(2) = j - \frac{1}{2}\mathrm{sgn}(\kappa), \tag{17}$$

respectively.

2.3. Spherical Symmetry

The spherical RHB equation was solved in coordinate space in the RCHB theory. With spherical symmetry, the quasiparticle wave function in coordinate space can be written as

$$U_k = \frac{1}{r}\begin{pmatrix} iG^k_U(r)\mathcal{Y}^l_{\kappa m}(\Omega, s) \\ F^k_U(r)(\boldsymbol{\sigma}\cdot\hat{\boldsymbol{r}})\mathcal{Y}^l_{\kappa m}(\Omega, s) \end{pmatrix}\chi_t(t), \;\; V_k = \frac{1}{r}\begin{pmatrix} iG^k_V(r)\mathcal{Y}^l_{\kappa m}(\Omega, s) \\ F^k_V(r)(\boldsymbol{\sigma}\cdot\hat{\boldsymbol{r}})\mathcal{Y}^l_{\kappa m}(\Omega, s) \end{pmatrix}\chi_t(t), \tag{18}$$

where G and F are radial wave functions and χ_t is the isospin wave function. The angular part can be dealt with analytically, and the RHB equation is reduced to a set of integral-differential equations for radial wave functions [35],

$$\begin{aligned}
&\frac{dG_U(r)}{dr} + \frac{\kappa}{r}G_U(r) - (E + \lambda - V(r) + S(r))F_U(r) + r\int r'dr'\Delta_F(r, r')F_V(r') = 0, \\
&\frac{dF_U(r)}{dr} - \frac{\kappa}{r}F_U(r) + (E + \lambda - V(r) - S(r))G_U(r) + r\int r'dr'\Delta_G(r, r')G_V(r') = 0, \\
&\frac{dG_V(r)}{dr} + \frac{\kappa}{r}G_V(r) + (E - \lambda + V(r) - S(r))F_V(r) + r\int r'dr'\Delta_F(r, r')F_U(r') = 0, \\
&\frac{dF_V(r)}{dr} - \frac{\kappa}{r}F_V(r) - (E - \lambda + V(r) + S(r))G_V(r) + r\int r'dr'\Delta_G(r, r')G_U(r') = 0,
\end{aligned} \tag{19}$$

which can be solved using the shooting method with Runge—Kutta algorithms. These quasiparticle wave functions can be used to calculate various densities (8) and the pairing tensor so as to construct new potentials (6,7) and the pairing field (9) during the iterative solution of the RHB equation. With spherical symmetry, all these quantities only depend on the radial coordinate r such that the solving process is largely simplified.

2.4. Axial Symmetry

The axial RHB equation was solved in the DWS basis in the DRHBc theory. With the DWS basis, solving the RHB equation is equivalent to the diagonalization of the RHB matrix. For axially deformed nuclei with spatial reflection symmetry, π and m are good quantum numbers. Therefore, the RHB matrix can be decomposed into different m^π blocks. Moreover, because of time-reversal symmetry, one only needs to diagonalize the RHB matrix in each positive-m block,

$$\begin{pmatrix} \mathcal{A} - \lambda_\tau & \mathcal{B} \\ \mathcal{B}^\dagger & -\mathcal{A}^* + \lambda_\tau \end{pmatrix}\begin{pmatrix} \mathcal{U}_k \\ \mathcal{V}_k \end{pmatrix} = E_k \begin{pmatrix} \mathcal{U}_k \\ \mathcal{V}_k \end{pmatrix}, \tag{20}$$

where the matrix elements are

$$\mathcal{A} = h^{(m)}_{D(n\kappa)(n'\kappa')} = \langle n\kappa m|h_D|n'\kappa' m\rangle, \tag{21}$$

$$\mathcal{B} = \Delta^{(m)}_{(n\kappa)(n'\kappa')} = \langle n\kappa m|\Delta|\overline{n'\kappa' m}\rangle. \tag{22}$$

Details for the calculation of RHB matrix elements can be found in Ref. [40]. Note that for odd–mass or odd–odd nuclei, the equal filling approximation that conserves time-reversal symmetry is often adopted [41,54,74].

The obtained eigenvectors from the diagonalization process correspond to the expansion coefficients of quasiparticle wave functions in the DWS basis

$$\mathcal{U}_k = (u^{(m)}_{k,(n\kappa)}), \quad \mathcal{V}_k = (v^{(m)}_{k,(n\kappa)}). \tag{23}$$

From these coefficients and the basis wave functions, new densities and potentials can be calculated, which are axially deformed and expanded in terms of Legendre polynomials in the DRHBc theory [39,40,75],

$$f(\boldsymbol{r}) = \sum_{\lambda} f_\lambda(r) P_\lambda(\cos\theta), \quad \lambda = 0, 2, 4, \cdots, \tag{24}$$

with

$$f_\lambda(r) = \frac{2\lambda+1}{4\pi} \int d\Omega f(\boldsymbol{r}) P_\lambda(\Omega). \tag{25}$$

They only depend on the radial coordinate r and the polar angle θ because of axial symmetry. The expansion order λ is restricted to be even numbers due to the spatial reflection symmetry, which will be explained below.

2.5. Triaxial Symmetry

The triaxial RHB equation has been solved in the DWS basis in the TRHBc theory. In this case, m is no longer a quantum number due to the breaking of axial symmetry. Therefore, the RHB matrix is decomposed into $\pi = +$ and $\pi = -$ blocks.

The triaxially deformed densities and potentials depend on not only r and θ but also the azimuth angle φ. They are expanded in terms of spherical harmonic functions in the TRHBc theory,

$$f(\boldsymbol{r}) = \sum_{\lambda\mu} f_{\lambda\mu}(r) Y_{\lambda\mu}(\theta, \varphi), \quad \lambda = 0, 1, 2, \cdots, \quad \mu = -\lambda, -\lambda+1, \cdots, \lambda. \tag{26}$$

Symmetry analysis can provide limitations on the expansion orders λ and μ in Equation (26). Under the spatial reflection transformation,

$$\begin{aligned} \hat{P} f(\boldsymbol{r}) &= \hat{P} \sum_{\lambda\mu} f_{\lambda\mu}(r) Y_{\lambda\mu}(\theta, \varphi) \\ &= \sum_{\lambda\mu} f_{\lambda\mu}(r) Y_{\lambda\mu}(\pi - \theta, \pi + \varphi) \\ &= \sum_{\lambda\mu} f_{\lambda\mu}(r) (-1)^\lambda Y_{\lambda\mu}(\theta, \varphi). \end{aligned} \tag{27}$$

Therefore, the spatial reflection symmetry limits λ to being even numbers. This limitation also applies to Equation (24). Under the mirror transformation with respect to the xy plane,

$$\begin{aligned}\hat{P}_z V(\boldsymbol{r}) &= \hat{P}_z \sum_{\lambda\mu} f_{\lambda\mu}(r) Y_{\lambda\mu}(\theta,\varphi) \\ &= \sum_{\lambda\mu} f_{\lambda\mu}(r) Y_{\lambda\mu}(\pi-\theta,\varphi) \\ &= \sum_{\lambda\mu} f_{\lambda\mu}(r)(-1)^{\lambda+\mu} Y_{\lambda\mu}(\theta,\varphi).\end{aligned} \tag{28}$$

Therefore, the mirror symmetry with respect to the xy plane limits $\lambda+\mu$ to being even numbers. Considering the limitation on λ by the spatial reflection symmetry, here μ can also only be even numbers. Under the mirror transformation with respect to the yz plane,

$$\begin{aligned}\hat{P}_x V(\boldsymbol{r}) &= \hat{P}_x \sum_{\lambda\mu} f_{\lambda\mu}(r) Y_{\lambda\mu}(\theta,\varphi) \\ &= \sum_{\lambda\mu} f_{\lambda\mu}(r) Y_{\lambda\mu}(\theta,\pi-\varphi) \\ &= \sum_{\lambda\mu} f_{\lambda\mu}(r) Y_{\lambda-\mu}(\theta,\varphi).\end{aligned} \tag{29}$$

Therefore, the mirror symmetry with respect to the yz plane limits the $+\mu$ component to the same as the $-\mu$ one, i.e., $f_{\lambda\mu}(r) = f_{\lambda-\mu}(r)$. The mirror symmetry with respect to the xz plane also gives this limitation, because these symmetries are not independent; they satisfy $\hat{P} = \hat{P}_x\hat{P}_y\hat{P}_z$. Finally, for triaxial nuclei, the expansion (26) can be simplified by symmetry analysis as

$$\begin{aligned}f(\boldsymbol{r}) &= f_{00}(r)Y_{00}(\Omega) + \sum_{\lambda=2,4,\cdots}^{\mu=2,4,\cdots,\lambda} f_{\lambda\mu}(r)[Y_{\lambda\mu}(\Omega) + Y_{\lambda-\mu}(\Omega)] \\ &= f_{00}(r)Y_{00}(\Omega) + \sum_{\lambda=2,4,\cdots}^{\mu=2,4,\cdots,\lambda} 2f_{\lambda\mu}(r)\mathrm{Re}[Y_{\lambda\mu}(\Omega)].\end{aligned} \tag{30}$$

3. Applications to Halo Nuclei

3.1. The RCHB Theory

Since the discovery of the neutron halo in ^{11}Li, considerable efforts have been devoted to describing this nucleus in a microscopic way. Based on the Skyrme–Hartree–Fock [76,77] and the relativistic mean field [78] models, a qualitative description of the observed halo features in ^{11}Li could be achieved by an ad hoc renormalization of the mean-field potential to reproduce the neutron separation energies or the radius. A three-body quasiparticle continuum random-phase approximation calculation [79] takes into account the pairing correlations and quantitatively reproduces the radius of ^{11}Li, but a structureless core of ^{9}Li that neglects polarization effects is assumed. A fully self-consistent description of ^{11}Li is achieved by the RCHB theory [14], which takes into account the pairing correlations and continuum effects.

With the density functional NL2 and a zero-range density-dependent pairing force, the RCHB theory reproduces both the binding energies and the matter radii for Li isotopes. As shown in Figure 2, the RCHB calculated neutron density distribution for ^{11}Li is much more diffuse than that of ^{9}Li and reproduces the experimental results within uncertainties. The neutron halo in ^{11}Li contributes to the long tail of its density distribution and causes the sudden increase in the radius.

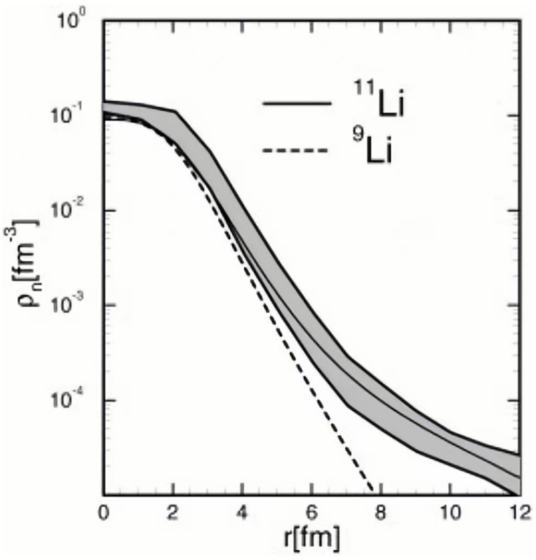

Figure 2. Calculated and experimental density distributions in ^{11}Li and ^{9}Li. The solid line shows the result of ^{11}Li, while the dashed line corresponds to the calculation of ^{9}Li. The shaded area gives the experimental results with error bars. Taken from Ref. [14].

A microscopic study of the single-particle levels in the canonical basis for ^{11}Li reveals that the pairing correlations cause a partial occupation of the very weakly bound $\nu 1p_{1/2}$ orbital and the $\nu 2s_{1/2}$ orbital embedded in the continuum. By analyzing the rms radii of different orbitals and their contributions to the total rms radius, it was found that the $2s_{1/2}$ orbital plays a crucial role in the formation of the neutron halo in ^{11}Li. More detailed results and discussion can be found in Ref. [14].

3.2. The DRHBc Theory

Around 2000, halos in deformed nuclei began to attract increasing attention. However, there had been controversy over the existence of deformed halos. The calculation based on a spherical Woods–Saxon potential suggests that all drip-line nuclei are spherical [80]. The calculation based on an axially deformed Woods–Saxon potential raises doubt about the existence of deformed halos because the $s_{1/2}$ component becomes overwhelmingly dominant in the wavefunctions of $m^\pi = 1/2^+$ orbitals as their binding energies approach zero [81]. The calculation based on a three-body model indicates that it is unlikely to find deformed halo nuclei near the dripline because the correlations between nucleons and those due to the deformation/excitation of the core inhibit the formation of halos [82]. To resolve the controversy, the experimental evidence and further theoretical investigations based on microscopic nuclear models are indispensable. In 2010, the DRHBc theory was developed, which self-consistently considers the axial deformation, pairing correlations, and continuum effects [39]. The deformed halos in neutron-rich magnesium isotopes are predicted and the shape decoupling between the core and the halo is illustrated by the DRHBc theory [39,40]. Later, the experimental evidence for deformed halo nuclei ^{31}Ne [83] and ^{37}Mg [84,85] was reported in 2014.

Figure 3 shows the DRHBc calculated density distributions for ^{44}Mg with the density functional NL3. In Figure 3a, owing to the large neutron excess, the neutron density extends much farther in space than the proton density and shows a halo structure. The neutron density is decomposed into the contribution of the core in Figure 3b and that of the halo in Figure 3c. The core is prolate while the halo has an oblate deformation, which is so-called shape decoupling. This shape decoupling is considered an interesting phenomenon near the dripline to be detected in future experiments [86]. Details on the prediction of the neutron halo and shape decoupling in ^{44}Mg can be found in Ref. [39].

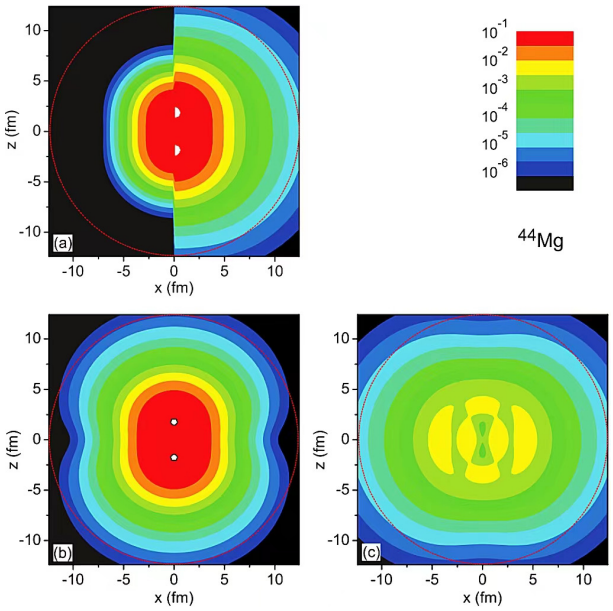

Figure 3. Density distributions of ^{44}Mg with the z axis as the symmetry axis. (**a**) The proton density (for $x < 0$) and the neutron density (for $x > 0$); (**b**) the density of the neutron core; and (**c**) the density of the neutron halo. In each plot, a dotted circle is drawn to guide the eye. Taken from Ref. [39].

Although magnesium isotopes heavier than ^{40}Mg are yet to be produced in the laboratory [87] and the prediction is to be verified, the DRHBc description is in good agreement with the existing data of binding energies, neutron separation energies, matter radii, and quadrupole deformations for magnesium isotopes [40,48,53]. Recently, the DRHBc theory achieved a microscopic, self-consistent, and density-functional independent description of the deformed p-wave neutron halo in ^{37}Mg [88].

3.3. The TRHBc Theory

Non-axial deformation, i.e., triaxial deformation, is one of the fundamental deformation degrees of freedom in atomic nuclei. Its importance has been demonstrated in nuclear fission [89], nuclear chirality [90], and wobbling motion [34]. Recently, the information on nuclear deformation has been extracted from relativistic heavy-ion collision experiments [91], and the evidence of the triaxial structure in ^{129}Xe has been revealed at the CERN Large Hadron Collider [92], which greatly stimulates research interest in triaxial nuclei. The existence of the halo phenomenon in triaxial nuclei is an interesting but less explored topic. In 2021, calculations based on Woods–Saxon potentials pointed out that the region of halo nuclei might be extended because the triaxial deformation allows the appearance of s or p wave components in some weakly bound orbitals [93]. In 2022, the TRHBc theory was developed, which considers the triaxial deformation, pairing correlations, and continuum effects in a microscopic and self-consistent way [55]. The TRHBc theory has predicted that ^{42}Al is a triaxial halo nucleus and there is a novel shape decoupling on the triaxial level between its core and halo.

The experimental proton drip line and the available data of neutron separation energies and charge radii for aluminum isotopes are well reproduced by the TRHBc theory with the density functionals PC-PK1, NL3*, NL-SH, and PK1. The neutron-richest odd–odd aluminum isotope observed so far, ^{42}Al [87], is predicted to be triaxially deformed with $\beta = 0.35$ and $\gamma = 42°$. Its one-neutron separation energy is predicted to be 0.68 MeV, in agreement with the AME2020 [94], and the neutron rms radius is 3.94 fm, remarkably larger than the empirical value. Figure 4 displays the neutron density distributions in different planes contributed by the core and the halo of ^{42}Al. It can clearly be seen that the halo density extends much farther than the core, particularly in the yz plane, supporting a triaxial halo. Quantitatively, the rms radii are 5.26 fm for the halo and 3.85 fm for the

core; the deformation parameters (β, γ) are (0.79, -23°) for the halo and (0.38, 50°) for the core. Here, the negative value of γ for the halo means that the y axis is the intermediate axis while x is the short one, which is just the reverse of the case for the core. With the corresponding rms radius, β and γ, schematic pictures are also given in Figure 4, where the short, intermediate, and long axes can be clearly distinguished. The novel shape decoupling between the core and the halo in ^{42}Al includes the change in the deformation and the exchange of the intermediate and short axes. More detailed results and discussions on exploring triaxial halo nuclei can be found in Ref. [55].

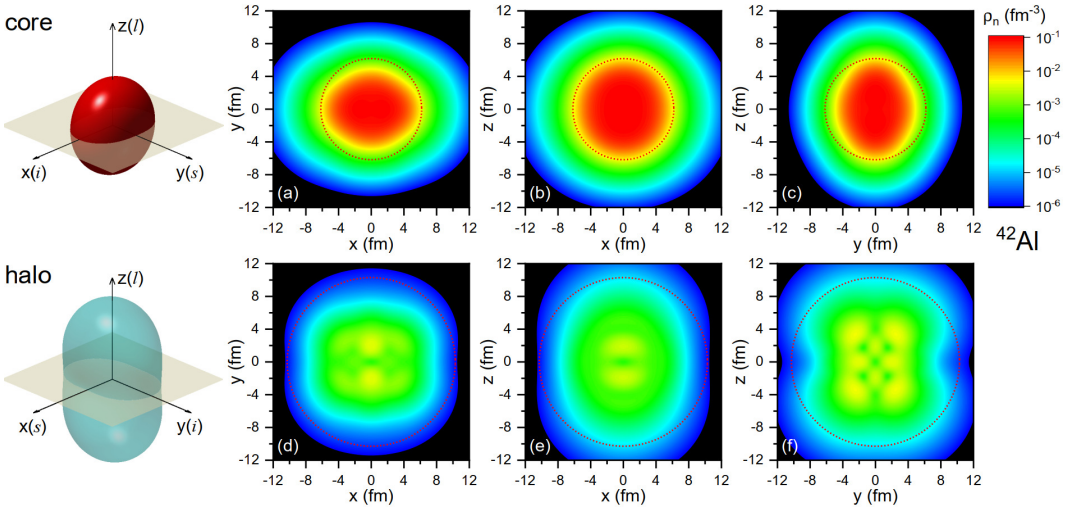

Figure 4. Neutron density distributions in xy, xz, and yz planes contributed by the core (**a**–**c**) and the halo (**d**–**f**) of ^{42}Al. In each plot, a circle in a dotted line is drawn to guide the eye. With the rms radius and deformation parameters, β and γ from the densities, the corresponding schematic shapes for the core and the halo are given in the left, in which s, i, and l, respectively, represent the short, intermediate, and long axes. Taken from Ref. [55].

4. Summary and Prospect

Since the discovery of the halo phenomenon in ^{11}Li, the study of halo nuclei has always been one of the most important topics in both experimental and theoretical nuclear physics. In tandem with advancements in experimental investigation, the CDFT has achieved great success in describing and predicting halo nuclei. Based on spherical symmetry, the RCHB theory has described the first halo nucleus ^{11}Li self-consistently and predicted the giant halo phenomenon. Based on axial symmetry, the DRHBc theory has many applications to deformed halo nuclei, including the prediction of deformed halo nuclei ^{39}Na and ^{42,44}Mg and the shape decoupling phenomena therein, the description of deformed halo nuclei ^{17,19}B, ^{15,19,22}C, ^{31}Ne, and ^{37}Mg, etc. Based on triaxial symmetry, the TRHBc theory has been recently developed and applied to explore halos in triaxially deformed nuclei. In this paper, the basic framework of the CDFT, the methodology for solving the RHB equation, and the roles of symmetries in simplifying the formalism of the RCHB, DRHBc, and TRHBc theories are presented in Section 2. The background of the development of these theories and their first applications to spherical (^{11}Li), axially deformed (^{44}Mg), and triaxially deformed (^{42}Al) halo nuclei are introduced in Section 3.

The shape decoupling between the core and the halo in deformed halo nuclei immediately attracted the attention of experimental physicists once predicted [86]. Its concept was further extended beyond the originally proposed prolate–oblate shape decoupling to those on the triaxial [55] and higher-order deformation (e.g., hexadecapole) [88] levels. However, the experimental manifestations associated with shape decoupling phenomena were not yet identified. It is hoped that the future precise measurements of nuclear density distributions or scattering experiments utilizing hadronic probes will unravel the mystery surrounding shape decoupling in deformed halo nuclei.

How can the excited states in halo nuclei be described? In 2021, the AMP method was implemented in the DRHBc theory to explore the rotational excitation of deformed halo nuclei [95,96]. The ground-state rotational bands of ^{36,38,40}Mg are reproduced reasonably well [96], and it has been demonstrated that the deformed halo structure persists from the ground state in the intrinsic frame to collective states [95]. In 2022, the finite amplitude method (FAM) based on the DRHBc theory was developed and applied to study the isoscalar giant monopole resonance of even–even nuclei in the calcium isotopic chain [97], where giant halos were predicted near the neutron dripline about twenty years ago [98,99]. Due to the advantages of the DRHBc theory in describing exotic nuclei, the DRHBc-FAM calculated results are closer to the energy-weighted sum rule than the calculations on the HO basis [97]. The DRHBc theory was also extended to go beyond the mean-field framework by performing the two-dimensional collective Hamiltonian [100], which paves an alternative means of investigating the collective states in halo nuclei. Similarly, these approaches can be developed based on the new TRHBc theory, enabling the future exploration of rotational bands, vibrational excitations, and shape transitions in triaxial halo nuclei.

Author Contributions: Conceptualization, K.Z.; writing—original draft preparation, Y.X., Q.L. and K.Z.; writing—review and editing, S.Y. and K.Z. All authors have read and agreed to the published version of the manuscript.

Funding: This research was funded by the National Natural Science Foundation of China under grants U2230207 and U2030209 and the National Key Program for Research and Development of China under grants 2020YFA0406001 and 2020YFA0406002.

Data Availability Statement: No new data were created or analyzed in this study. Data sharing is not applicable to this article.

Acknowledgments: We acknowledge supports from H. Yan. One of the authors (K.Y.Z.) expresses their gratitude to L.S. Geng, J. Meng, C. Pan, P. Ring, B.H. Sun, X.-X. Sun, D. Vretenar, S.Q. Zhang, S.S. Zhang, P.W. Zhao, S.-G. Zhou, and the members of the DRHBc Mass Table Collaboration for the helpful discussions.

Conflicts of Interest: The authors declare no conflict of interest.

Abbreviations

The following abbreviations are used in this manuscript:

CDFT	Covariant density functional theory
RCHB theory	Relativistic continuum Hartree–Bogoliubov theory
DRHBc theory	Deformed relativistic Hartree–Bogoliubov theory in continuum
TRHBc theory	Triaxial relativistic Hartree–Bogoliubov theory in continuum
HO basis	Harmonic oscillator basis
SWS basis	Schrödinger Woods–Saxon basis
DWS basis	Dirac Woods–Saxon basis
AMP	Angular momentum projection
FAM	Finite amplitude method

References

1. Tanihata, I.; Hamagaki, H.; Hashimoto, O.; Shida, Y.; Yoshikawa, N.; Sugimoto, K.; Yamakawa, O.; Kobayashi, T.; Takahashi, N. Measurements of Interaction Cross Sections and Nuclear Radii in the Light *p*-Shell Region. *Phys. Rev. Lett.* **1985**, *55*, 2676–2679. [CrossRef]
2. Kobayashi, T.; Yamakawa, O.; Omata, K.; Sugimoto, K.; Shimoda, T.; Takahashi, N.; Tanihata, I. Projectile Fragmentation of the Extremely Neutron-Rich Nucleus ^{11}Li at 0.79 GeV/nucleon. *Phys. Rev. Lett.* **1988**, *60*, 2599–2602. [CrossRef]
3. Tanihata, I.; Savajols, H.; Kanungo, R. Recent experimental progress in nuclear halo structure studies. *Prog. Part. Nucl. Phys.* **2013**, *68*, 215–313. [CrossRef]
4. Zhang, K.Y.; Papakonstantinou, P.; Mun, M.H.; Kim, Y.; Yan, H.; Sun, X.X. Collapse of the $N = 28$ shell closure in the newly discovered ^{39}Na nucleus and the development of deformed halos towards the neutron dripline. *Phys. Rev. C* **2023**, *107*, L041303. [CrossRef]

5. Zhukov, M.; Danilin, B.; Fedorov, D.; Bang, J.; Thompson, I.; Vaagen, J. Bound state properties of Borromean halo nuclei: ^{6}He and ^{11}Li. *Phys. Rep.* **1993**, *231*, 151–199. [CrossRef]
6. Hansen, P.G.; Jensen, A.S.; Jonson, B. Nuclear Halos. *Annu. Rev. Nuc. Part. Sci.* **1995**, *45*, 591–634. [CrossRef]
7. Otsuka, T.; Fukunishi, N.; Sagawa, H. Structure of exotic neutron-rich nuclei. *Phys. Rev. Lett.* **1993**, *70*, 1385–1388. [CrossRef] [PubMed]
8. Kuo, T.T.S.; Krmpotić, F.; Tzeng, Y. Suppression of Core Polarization in Halo Nuclei. *Phys. Rev. Lett.* **1997**, *78*, 2708–2711. [CrossRef]
9. Horiuchi, H.; Kanada-En'yo, Y.; Ono, A. Neutron-rich nuclei studied with AMD. *Z. Phys. A* **1994**, *349*, 279–283. [CrossRef]
10. Itagaki, N.; Aoyama, S. Systematic study on He isotopes with the antisymmetrized molecular dynamics plus generator coordinate method. *Phys. Rev. C* **1999**, *61*, 024303. [CrossRef]
11. Ryberg, E.; Forssén, C.; Hammer, H.W.; Platter, L. Effective field theory for proton halo nuclei. *Phys. Rev. C* **2014**, *89*, 014325. [CrossRef]
12. Ji, C.; Elster, C.; Phillips, D.R. ^{6}He nucleus in halo effective field theory. *Phys. Rev. C* **2014**, *90*, 044004. [CrossRef]
13. Terasaki, J.; Heenen, P.H.; Flocard, H.; Bonche, P. 3D solution of Hartree-Fock-Bogoliubov equations for drip-line nuclei. *Nucl. Phys. A* **1996**, *600*, 371–386. [CrossRef]
14. Meng, J.; Ring, P. Relativistic Hartree-Bogoliubov Description of the Neutron Halo in ^{11}Li. *Phys. Rev. Lett.* **1996**, *77*, 3963–3966. [CrossRef]
15. Bender, M.; Heenen, P.H.; Reinhard, P.G. Self-consistent mean-field models for nuclear structure. *Rev. Mod. Phys.* **2003**, *75*, 121–180. [CrossRef]
16. Ren, Z.X.; Zhao, P.W. Toward a bridge between relativistic and nonrelativistic density functional theories for nuclei. *Phys. Rev. C* **2020**, *102*, 021301. [CrossRef]
17. Ginocchio, J.N. Pseudospin as a Relativistic Symmetry. *Phys. Rev. Lett.* **1997**, *78*, 436–439. [CrossRef]
18. Meng, J.; Sugawara-Tanabe, K.; Yamaji, S.; Ring, P.; Arima, A. Pseudospin symmetry in relativistic mean field theory. *Phys. Rev. C* **1998**, *58*, R628–R631. [CrossRef]
19. Meng, J.; Sugawara-Tanabe, K.; Yamaji, S.; Arima, A. Pseudospin symmetry in Zr and Sn isotopes from the proton drip line to the neutron drip line. *Phys. Rev. C* **1999**, *59*, 154–163. [CrossRef]
20. Chen, T.S.; Lu, H.F.; Meng, J.; Zhang, S.Q.; Zhou, S.G. Pseudospin symmetry in relativistic framework with harmonic oscillator potential and Woods-Saxon potential. *Chin. Phys. Lett.* **2003**, *20*, 358.
21. Ginocchio, J.N. Relativistic symmetries in nuclei and hadrons. *Phys. Rep.* **2005**, *414*, 165–261. [CrossRef]
22. Liang, H.; Meng, J.; Zhou, S.G. Hidden pseudospin and spin symmetries and their origins in atomic nuclei. *Phys. Rep.* **2015**, *570*, 1–84. [CrossRef]
23. Zhou, S.G.; Meng, J.; Ring, P. Spin Symmetry in the Antinucleon Spectrum. *Phys. Rev. Lett.* **2003**, *91*, 262501. [CrossRef] [PubMed]
24. He, X.T.; Zhou, S.G.; Meng, J.; Zhao, E.G.; Scheid, W. Test of spin symmetry in anti-nucleon spectra. *Eur. Phys. J. A* **2006**, *28*, 265–269. [CrossRef]
25. Koepf, W.; Ring, P. A relativistic description of rotating nuclei: The yrast line of ^{20}Ne. *Nucl. Phys. A* **1989**, *493*, 61–82. [CrossRef]
26. Ring, P. Relativistic mean field theory in finite nuclei. *Prog. Part. Nucl. Phys.* **1996**, *37*, 193–263. [CrossRef]
27. Vretenar, D.; Afanasjev, A.V.; Lalazissis, G.A.; Ring, P. Relativistic Hartree-Bogoliubov theory: Static and dynamic aspects of exotic nuclear structure. *Phys. Rep.* **2005**, *409*, 101–259. [CrossRef]
28. Meng, J.; Toki, H.; Zhou, S.G.; Zhang, S.Q.; Long, W.H.; Geng, L.S. Relativistic Continuum Hartree Bogoliubov theory for ground state properties of exotic nuclei. *Prog. Part. Nucl. Phys.* **2006**, *57*, 470–563. [CrossRef]
29. Nikšić, T.; Vretenar, D.; Ring, P. Relativistic nuclear energy density functionals: Mean-field and beyond. *Prog. Part. Nucl. Phys.* **2011**, *66*, 519–548. [CrossRef]
30. Meng, J.; Peng, J.; Zhang, S.Q.; Zhao, P.W. Progress on tilted axis cranking covariant density functional theory for nuclear magnetic and antimagnetic rotation. *Front. Phys.* **2013**, *8*, 55–79. [CrossRef]
31. Meng, J.; Zhou, S.G. Halos in medium-heavy and heavy nuclei with covariant density functional theory in continuum. *J. Phys. G* **2015**, *42*, 093101. [CrossRef]
32. Zhou, S.G. Multidimensionally constrained covariant density functional theories—Nuclear shapes and potential energy surfaces. *Phys. Scr.* **2016**, *91*, 063008–21. [CrossRef]
33. Meng, J.; Zhao, P. Relativistic density functional theory in nuclear physics. *AAPPS Bull.* **2021**, *31*, 2. [CrossRef]
34. Bohr, A.; Mottelson, B.R. *Nuclear Structure*; Benjamin: New York, NY, USA, 1975; Volume II.
35. Meng, J. Relativistic continuum Hartree-Bogoliubov theory with both zero range and finite range Gogny force and their application. *Nucl. Phys. A* **1998**, *635*, 3–42. [CrossRef]
36. Meng, J.; Ring, P. Giant Halo at the Neutron Drip Line. *Phys. Rev. Lett.* **1998**, *80*, 460–463. [CrossRef]
37. Lü, H.F.; Meng, J.; Zhang, S.Q.; Zhou, S.G. Neutron halos in hypernuclei. *Eur. Phys. J. A* **2003**, *17*, 19–24. [CrossRef]
38. Xia, X.W.; Lim, Y.; Zhao, P.W.; Liang, H.Z.; Qu, X.Y.; Chen, Y.; Liu, H.; Zhang, L.F.; Zhang, S.Q.; Kim, Y.; et al. The limits of the nuclear landscape explored by the relativistic continuum Hartree-Bogoliubov theory. *Atom. Data Nucl. Data Tabl.* **2018**, *121–122*, 1–215. [CrossRef]
39. Zhou, S.G.; Meng, J.; Ring, P.; Zhao, E.G. Neutron halo in deformed nuclei. *Phys. Rev. C* **2010**, *82*, 011301. [CrossRef]

40. Li, L.; Meng, J.; Ring, P.; Zhao, E.G.; Zhou, S.G. Deformed relativistic Hartree-Bogoliubov theory in continuum. *Phys. Rev. C* **2012**, *85*, 024312. [CrossRef]
41. Li, L.; Meng, J.; Ring, P.; Zhao, E.G.; Zhou, S.G. Odd systems in deformed relativistic Hartree-Bogoliubov theory in continuum. *Chin. Phys. Lett.* **2012**, *29*, 042101. [CrossRef]
42. Chen, Y.; Li, L.; Liang, H.; Meng, J. Density-dependent deformed relativistic Hartree-Bogoliubov theory in continuum. *Phys. Rev. C* **2012**, *85*, 067301. [CrossRef]
43. Yang, Z.H.; Kubota, Y.; Corsi, A.; Yoshida, K.; Sun, X.X.; Li, J.G.; Kimura, M.; Michel, N.; Ogata, K.; Yuan, C.X.; et al. Quasifree Neutron Knockout Reaction Reveals a Small *s*-Orbital Component in the Borromean Nucleus ^{17}B. *Phys. Rev. Lett.* **2021**, *126*, 082501. [CrossRef]
44. Sun, X.X. Deformed two-neutron halo in ^{19}B. *Phys. Rev. C* **2021**, *103*, 054315. [CrossRef]
45. Sun, X.X.; Zhao, J.; Zhou, S.G. Shrunk halo and quenched shell gap at $N = 16$ in ^{22}C: Inversion of *sd* states and deformation effects. *Phys. Lett. B* **2018**, *785*, 530. [CrossRef]
46. Sun, X.X.; Zhao, J.; Zhou, S.G. Study of ground state properties of carbon isotopes with deformed relativistic Hartree-Bogoliubov theory in continuum. *Nucl. Phys. A* **2020**, *1003*, 122011. [CrossRef]
47. Zhong, S.Y.; Zhang, S.S.; Sun, X.X.; Smith, M.S. Study of the deformed halo nucleus ^{31}Ne with Glauber model based on microscopic self-consistent structures. *Sci. China Phys. Mech. Astron.* **2022**, *65*, 262011. [CrossRef]
48. Zhang, K.Y.; Wang, D.Y.; Zhang, S.Q. Effects of pairing, continuum, and deformation on particles in the classically forbidden regions for Mg isotopes. *Phys. Rev. C* **2019**, *100*, 034312. [CrossRef]
49. Zhang, K.; Cheoun, M.K.; Choi, Y.B.; Chong, P.S.; Dong, J.; Geng, L.; Ha, E.; He, X.; Heo, C.; Ho, M.C.; et al. Deformed relativistic Hartree-Bogoliubov theory in continuum with a point-coupling functional: Examples of even-even Nd isotopes. *Phys. Rev. C* **2020**, *102*, 024314. [CrossRef]
50. Zhang, K.; He, X.; Meng, J.; Pan, C.; Shen, C.; Wang, C.; Zhang, S. Predictive power for superheavy nuclear mass and possible stability beyond the neutron drip line in deformed relativistic Hartree-Bogoliubov theory in continuum. *Phys. Rev. C* **2021**, *104*, L021301. [CrossRef]
51. Pan, C.; Zhang, K.Y.; Chong, P.S.; Heo, C.; Ho, M.C.; Lee, J.; Li, Z.P.; Sun, W.; Tam, C.K.; Wong, S.H.; et al. Possible bound nuclei beyond the two-neutron drip line in the $50 \leq Z \leq 70$ region. *Phys. Rev. C* **2021**, *104*, 024331. [CrossRef]
52. He, X.T.; Wang, C.; Zhang, K.Y.; Shen, C.W. Possible existence of bound nuclei beyond neutron drip lines driven by deformation. *Chin. Phys. C* **2021**, *45*, 101001. [CrossRef]
53. Zhang, K.; Cheoun, M.K.; Choi, Y.B.; Chong, P.S.; Dong, J.; Dong, Z.; Du, X.; Geng, L.; Ha, E.; He, X.T.; et al. Nuclear mass table in deformed relativistic Hartree-Bogoliubov theory in continuum, I: Even–even nuclei. *Atom. Data Nucl. Data Tabl.* **2022**, *144*, 101488. [CrossRef]
54. Pan, C.; Cheoun, M.K.; Choi, Y.B.; Dong, J.; Du, X.; Fan, X.H.; Gao, W.; Geng, L.; Ha, E.; He, X.T.; et al. Deformed relativistic Hartree-Bogoliubov theory in continuum with a point-coupling functional. II. Examples of odd Nd isotopes. *Phys. Rev. C* **2022**, *106*, 014316. [CrossRef]
55. Zhang, K.Y.; Zhang, S.Q.; Meng, J. Possible neutron halo in triaxial nucleus ^{42}Al. *arXiv* **2022**, arXiv:2212.05703.
56. Meng, J. (Ed.) *Relativistic Density Functional for Nuclear Structure*; International Review of Nuclear Physics; World Scientific: Singapore, 2016; Volume 10.
57. Bürvenich, T.; Madland, D.G.; Maruhn, J.A.; Reinhard, P.G. Nuclear ground state observables and QCD scaling in a refined relativistic point coupling model. *Phys. Rev. C* **2002**, *65*, 044308. [CrossRef]
58. Long, W.H.; Ring, P.; Meng, J.; Van Giai, N.; Bertulani, C.A. Nuclear halo structure and pseudospin symmetry. *Phys. Rev. C* **2010**, *81*, 031302. [CrossRef]
59. Long, W.H.; Ring, P.; Giai, N.V.; Meng, J. Relativistic Hartree-Fock-Bogoliubov theory with density dependent meson-nucleon couplings. *Phys. Rev. C* **2010**, *81*, 024308. [CrossRef]
60. Geng, J.; Long, W.H. Relativistic Hartree-Fock-Bogoliubov model for axially deformed nuclei. *Phys. Rev. C* **2022**, *105*, 034329. [CrossRef]
61. Ring, P.; Schuck, P. *The Nuclear Many-Body Problem*; Springer: Berlin, Germany, 1980.
62. Meng, J. Pairing interaction in exotic nuclei: Finite range or zero range? *Phys. Rev. C* **1998**, *57*, 1229–1232. [CrossRef]
63. Tian, Y.; Ma, Z.; Ring, P. A finite range pairing force for density functional theory in superfluid nuclei. *Phys. Lett. B* **2009**, *676*, 44–50. [CrossRef]
64. Nikšić, T.; Paar, N.; Vretenar, D.; Ring, P. DIRHB—A relativistic self-consistent mean-field framework for atomic nuclei. *Comput. Phys. Comm.* **2014**, *185*, 1808–1821. .: 10.1016/j.cpc.2014.02.027. [CrossRef]
65. Stoitsov, M.V.; Nazarewicz, W.; Pittel, S. New discrete basis for nuclear structure studies. *Phys. Rev. C* **1998**, *58*, 2092–2098. [CrossRef]
66. Stoitsov, M.; Ring, P.; Vretenar, D.; Lalazissis, G.A. Solution of relativistic Hartree-Bogoliubov equations in configurational representation: Spherical neutron halo nuclei. *Phys. Rev. C* **1998**, *58*, 2086–2091. [CrossRef]
67. Zhang, Y.N.; Pei, J.C.; Xu, F.R. Hartree-Fock-Bogoliubov descriptions of deformed weakly bound nuclei in large coordinate spaces. *Phys. Rev. C* **2013**, *88*, 054305. [CrossRef]
68. Pöschl, W.; Vretenar, D.; Lalazissis, G.A.; Ring, P. Relativistic Hartree-Bogoliubov Theory with Finite Range Pairing Forces in Coordinate Space: Neutron Halo in Light Nuclei. *Phys. Rev. Lett.* **1997**, *79*, 3841–3844. [CrossRef]

69. Zhou, S.G.; Meng, J.; Yamaji, S.; Yang, S.C. Deformed relativistic Hartree theory in coordinate space and in harmonic oscillator basis. *Chin. Phys. Lett.* **2000**, *17*, 717. [CrossRef]
70. Zhou, S.G.; Meng, J.; Ring, P. Spherical relativistic Hartree theory in a Woods-Saxon basis. *Phys. Rev. C* **2003**, *68*, 034323. [CrossRef]
71. Schunck, N.; Egido, J.L. Nuclear halos and drip lines in symmetry-conserving continuum Hartree-Fock-Bogoliubov theory. *Phys. Rev. C* **2008**, *78*, 064305. [CrossRef]
72. Geng, J.; Xiang, J.; Sun, B.Y.; Long, W.H. Relativistic Hartree-Fock model for axially deformed nuclei. *Phys. Rev. C* **2020**, *101*, 064302. [CrossRef]
73. Zhang, K.Y.; Pan, C.; Zhang, S.Q. Optimized Dirac Woods-Saxon basis for covariant density functional theory. *Phys. Rev. C* **2022**, *106*, 024302. [CrossRef]
74. Perez-Martin, S.; Robledo, L.M. Microscopic justification of the equal filling approximation. *Phys. Rev. C* **2008**, *78*, 014304. [CrossRef]
75. Pan, C.; Zhang, K.; Zhang, S. Multipole expansion of densities in the deformed relativistic Hartree-Bogoliubov theory in continuum. *Int. J. Mod. Phys. E* **2019**, *28*, 1950082. [CrossRef]
76. Bertsch, G.F.; Brown, B.A.; Sagawa, H. High-energy reaction cross sections of light nuclei. *Phys. Rev. C* **1989**, *39*, 1154–1157. [CrossRef]
77. Sagawa, H. Density distributions of halo nuclei. *Phys. Lett. B* **1992**, *286*, 7–12. [CrossRef]
78. Zhu, Z.; Shen, W.; Cai, Y.; Ma, Y. Study of halo nuclei with phenomenological relativistic mean field approach. *Phys. Lett. B* **1994**, *328*, 1–4. [CrossRef]
79. Bertsch, G.; Esbensen, H. Pair correlations near the neutron drip line. *Ann. Phys.* **1991**, *209*, 327–363. [CrossRef]
80. Tanihata, I.; Hirata, D.; Toki, H. Are all nucleus spherical at the drip line? *Nucl. Phys. A* **1995**, *583*, 769–774. [CrossRef]
81. Hamamoto, I. Dominance of low-ℓ component in weakly bound deformed single-neutron orbits. *Phys. Rev. C* **2004**, *69*, 041306. [CrossRef]
82. Nunes, F. Valence pairing, core deformation and the development of two-neutron halos. *Nucl. Phys. A* **2005**, *757*, 349–359. [CrossRef]
83. Nakamura, T.; Kobayashi, N.; Kondo, Y.; Satou, Y.; Tostevin, J.A.; Utsuno, Y.; Aoi, N.; Baba, H.; Fukuda, N.; Gibelin, J.; et al. Deformation-Driven *p*-Wave Halos at the Drip Line: ^{31}Ne. *Phys. Rev. Lett.* **2014**, *112*, 142501. [CrossRef] [PubMed]
84. Kobayashi, N.; Nakamura, T.; Kondo, Y.; Tostevin, J.A.; Utsuno, Y.; Aoi, N.; Baba, H.; Barthelemy, R.; Famiano, M.A.; Fukuda, N.; et al. Observation of a *p*-Wave One-Neutron Halo Configuration in ^{37}Mg. *Phys. Rev. Lett.* **2014**, *112*, 242501. [CrossRef] [PubMed]
85. Takechi, M.; Suzuki, S.; Nishimura, D.; Fukuda, M.; Ohtsubo, T.; Nagashima, M.; Suzuki, T.; Yamaguchi, T.; Ozawa, A.; Moriguchi, T.; et al. Evidence of halo structure in ^{37}Mg observed via reaction cross sections and intruder orbitals beyond the island of inversion. *Phys. Rev. C* **2014**, *90*, 061305. [CrossRef]
86. Cottle, P.D.; Kemper, K.W. A Work Along the Dripline. *Physics* **2012**, *5*, 49. [CrossRef]
87. Baumann, T.; Amthor, A.M.; Bazin, D.; Brown, B.A.; Folden, C.M., III; Gade, A.; Ginter, T.N.; Hausmann, M.; Matos, M.; Morrissey, D.J.; et al. Discovery of ^{40}Mg and ^{42}Al suggests neutron drip-line slant towards heavier isotopes. *Nature* **2007**, *449*, 1022–1024. [CrossRef]
88. Zhang, K.Y.; Yang, S.Q.; An, J.L.; Zhang, S.S.; Papakonstantinou, P.; Mun, M.H.; Kim, Y.; Yan, H. Missed prediction of the neutron halo in ^{37}Mg. *arXiv* **2023**, arXiv:2306.16011. https://doi.org/10.48550/arXiv.2306.16011.
89. Lu, B.N.; Zhao, E.G.; Zhou, S.G. Potential energy surfaces of actinide nuclei from a multidimensional constrained covariant density functional theory: Barrier heights and saddle point shapes. *Phys. Rev. C* **2012**, *85*, 011301. [CrossRef]
90. Frauendorf, S.; Meng, J. Tilted rotation of triaxial nuclei. *Nucl. Phys. A* **1997**, *617*, 131–147. [CrossRef]
91. Giacalone, G.; Jia, J.; Zhang, C. Impact of Nuclear Deformation on Relativistic Heavy-Ion Collisions: Assessing Consistency in Nuclear Physics across Energy Scales. *Phys. Rev. Lett.* **2021**, *127*, 242301. [CrossRef]
92. Bally, B.; Bender, M.; Giacalone, G.; Somà, V. Evidence of the Triaxial Structure of ^{129}Xe at the Large Hadron Collider. *Phys. Rev. Lett.* **2022**, *128*, 082301. [CrossRef]
93. Uzawa, K.; Hagino, K.; Yoshida, K. Role of triaxiality in deformed halo nuclei. *Phys. Rev. C* **2021**, *104*, L011303. [CrossRef]
94. Wang, M.; Huang, W.; Kondev, F.; Audi, G.; Naimi, S. The AME 2020 atomic mass evaluation (II). Tables, graphs and references. *Chin. Phys. C* **2021**, *45*, 030003. [CrossRef]
95. Sun, X.X.; Zhou, S.G. Rotating deformed halo nuclei and shape decoupling effects. *Sci. Bull.* **2021**, *66*, 2072–2078. [CrossRef]
96. Sun, X.X.; Zhou, S.G. Angular momentum projection in the deformed relativistic Hartree-Bogoliubov theory in continuum. *Phys. Rev. C* **2021**, *104*, 064319. [CrossRef]
97. Sun, X.; Meng, J. Finite amplitude method on the deformed relativistic Hartree-Bogoliubov theory in continuum: The isoscalar giant monopole resonance in exotic nuclei. *Phys. Rev. C* **2022**, *105*, 044312. [CrossRef]
98. Meng, J.; Toki, H.; Zeng, J.Y.; Zhang, S.Q.; Zhou, S.G. Giant halo at the neutron drip line in Ca isotopes in relativistic continuum Hartree-Bogoliubov theory. *Phys. Rev. C* **2002**, *65*, 041302. [CrossRef]

99. Zhang, S.Q.; Meng, J.; Zhou, S.G. Proton magic even-even isotopes and giant halos of Ca isotopes with relativistic continuum Hartree-Bogoliubov theory. *Sci. China Ser. G: Phys. Ast.* **2003**, *46*, 632–658. [CrossRef]
100. Sun, W.; Zhang, K.Y.; Pan, C.; Fan, X.H.; Zhang, S.; Li, Z.P. Beyond-mean-field dynamical correlations for nuclear mass table in deformed relativistic Hartree-Bogoliubov theory in continuum. *Chin. Phys. C* **2022**, *46*, 064103. [CrossRef]